

16. ROCK MAGNETIC STUDY OF SEDIMENTS FROM THE JAPAN TRENCH, ODP LEG 186: IMPLICATIONS FOR DEFORMATION OF SEDIMENTS¹

Toshiya Kanamatsu² and Kazue Matsuo³

ABSTRACT

The fabric of fine-grained sediments from the deep-sea terrace on the landward side of the Japan Trench, cored during Ocean Drilling Program Leg 186, was analyzed using the anisotropy of magnetic susceptibility. The purpose of this study was to document the magnetic fabrics formed in a tensional environment. Faults and joints (healed fractures) were found in the lower portion of recovered core. Analysis of these structures suggests an east-west tensional direction. The general shape of the magnetic fabric ellipsoid is fairly oblate. Bedding planes dip to the east in Hole 1151, and the magnetic fabric is completely controlled by the bedding plane. The magnetic fabric in the interval highly affected by fracturing, however, shows higher anisotropy. Magnetic foliations, which have been reorientated using paleomagnetic north, incline eastward and westward.

INTRODUCTION

Several recent studies have examined the sensitivity of anisotropy of magnetic susceptibility (AMS) in weakly deformed sediments from various environments. These studies have established that it is possible to distinguish important features of magnetic fabric and relate them to past tectonic events, especially in the compressive regimes (cf. Hounslow, 1990; Owens, 1993; Housen et al., 1996, Kanamatsu et al., 2001),

¹Kanamatsu, T., and Matsuo, K., 2003. Rock magnetic study of sediments from the Japan Trench, ODP Leg 186: implications for deformation of sediments. *In* Suyehiro, K., Sacks, I.S., Acton, G.D., and Oda, M. (Eds.), *Proc. ODP, Sci. Results*, 186, 1–21 [Online]. Available from World Wide Web: <http://www-odp.tamu.edu/publications/186_SR/VOLUME/CHAPTERS/113.PDF>. [Cited YYYY-MM-DD]

²Deep Sea Research Department, Japan Marine Science and Technology Center, 2-15 Natsushima-cho, Yokosuka, 237-0061 Japan.
toshiyak@jamstec.go.jp

³Japan Marine Works Ltd., Live Pier Kanazawahakkei, 1-1-7 2F Mutsuura, Kanazawaku, Yokohama, 236-0031, Japan.

Initial receipt: 2 January 2002

Acceptance: 7 August 2002

Web publication: 28 February 2003
Ms 186SR-113

which record systematic reorientation of original sedimentary fabric. The AMS method is now considered to be a useful marker in structural analysis of syndepositional to postdepositional weakly deformed sediments in a compressive tectonic setting. The magnetic lineations are often perpendicular to sigma 1.

The sedimentary sequence in the landward slope of the Japan Trench (Fig. F1) provides the opportunity to study AMS in the vicinity of a trench. The core recovered during Leg 186 has microfaults and joints (healed fractures) that were considered to have been formed by tensional environments (see "Structural Geology" in Shipboard Scientific Party, 2000a). AMS in tensional environments has not been studied very much, and the characteristics of magnetic fabric in such an environment is not clear. Here, we applied the AMS method to determine the features of the magnetic fabric and to evaluate its usefulness in tensional environments.

From the sedimentary sequence recovered during Leg 186, several lithostratigraphic units were identified (Shipboard Scientific Party, 2000a, 2000b). The four lithologic units defined for Site 1150 are

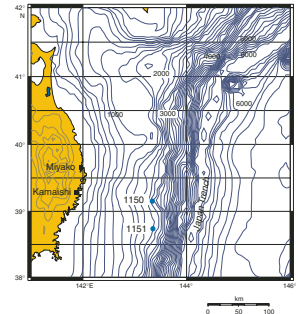
- Unit I (0–222.2 mbsf): hemipelagic diatomaceous ooze and hemipelagic diatomaceous clay with tephra,
- Unit II (222.2–598.0 mbsf): hemipelagic diatomaceous silty clay and clay,
- Unit III (598.0–1046.5 mbsf): hemipelagic diatomaceous silty claystone and clayey siltstone, and
- Unit IV (1046.5–1181.6 mbsf): diatomaceous silty claystone and clayey siltstone.

The five lithologic units defined for Site 1151 are

- Unit I (0–189.5 mbsf): homogeneous diatom-bearing silty clay and diatomaceous silty clay,
- Unit II (189.5–430.3 mbsf): hemipelagic siliceous sponge spicule-bearing diatomaceous silty clay and diatom-bearing diatomaceous silty clay,
- Unit III (430.3–896.75 mbsf): hemipelagic diatom-bearing silty clay,
- Unit IV (896.75–1007.4 mbsf): hemipelagic diatom and siliceous sponge spicule-bearing silty claystone, and
- Unit V (1007.4–1113.6 mbsf): hemipelagic glassy or glass-bearing silty claystone.

Brittle structures, faults and joints, are frequently found in these sedimentary sequences at Sites 1150 and 1151 below 600–700 meters below seafloor (mbsf) (Sacks, Suyehiro, Acton, et al., 2000). They were considered to have formed in tensional environments. The structures were generally healed and filled with fine-grained dark gray clay. The width of the infill varies from a few millimeters to a few tenths of a millimeter. No secondary mineralization or recrystallization was observed (Sacks, Suyehiro, Acton, et al., 2000). The structures are generally straight with sharp fault traces and steep dips. The observed displacement along the faults is typically only a few millimeters. Normal faults are most commonly observed as conjugated sets. Onboard analysis on the orientation of structures indicated that the dominant orientation was in east-southeast to west-northwest tensional direction.

F1. Location of Sites 1150 and 1151, p. 9.



METHODS

The AMS of sediment may be developed in two stages, depositional and postdepositional. The first stage occurs during settling of grains on the seafloor. During deposition, grains with a shape anisotropy tend to preferentially fall with their minimum axes perpendicular to the bedding plane. As a result, the fabric has an oblate shape (well-developed foliation). During postdepositional processes, the fabric may be affected by compaction, tectonic forces, bioturbation, or migration of fluid and gases. The AMS in rocks and sediments can be represented by a second-rank tensor ellipsoid. The three principal axes are expressed as K_{\max} = maximum susceptibility, K_{int} = intermediate susceptibility, and K_{\min} = minimum susceptibility. These provide two types of information that characterize fabric. The first is the directional information represented by the orientations of the three principal susceptibility axes (magnetic lineation; L). The second is the shape of the ellipsoid (magnetic foliation; F), which is defined by magnitudes of the principal susceptibility axes. In this paper, the following parameters were used to quantify the shape of the magnetic ellipsoids:

$$L = K_{\max}/K_{\text{int}} \text{ (Balsley and Buddington, 1960),}$$

$$F = K_{\text{int}}/K_{\min} \text{ (Stacey et al., 1960), and}$$

$$P = \exp \left(\text{SQR} \left\{ 2[\eta_1 - \eta_m]^2 + (\eta_2 - \eta_m)^2 + (\eta_3 - \eta_m)^2 \right\} \right) \text{ (Jelinek, 1981),}$$

where

$$\eta_1 = \ln K_{\max},$$

$$\eta_2 = \ln K_{\text{int}},$$

$$\eta_3 = \ln K_{\min}, \text{ and}$$

$$\eta_m = (\eta_1 + \eta_2 + \eta_3)/3.$$

We sampled sediment from Holes 1150 and 1151 using 7-cm³ plastic cubes in order to compare the magnetic fabric. A total of 990 samples were collected from both holes. Samples in this study were routinely taken from the center of the halved core to avoid drilling disturbance around the core liner. Fine sediments were chosen for this study, and no coarse-grained layers were sampled. The fine sediment was considered to be uniform in lithology, more susceptible to tectonic deformation, and suited for paleomagnetic studies. Layers containing deformation structures such as visible faults and joints were avoided because they tend to show localized effects. Measurements of magnetization were made using a horizontal 2-G cryogenic magnetometer (2-G Enterprises). Natural remanent magnetization (NRM) and demagnetization were routinely measured at levels of 2, 5, 7, 10, 15, 20, 25, 30, 35, 40, 50, and 60 mT, and, subsequently, anhysteretic remanent magnetization (ARM) was imparted in an 80-mT alternating field (AF) with a 0.1-mT biasing field. ARM was also measured after AF demagnetization of 5, 10, 20, 30, and 40 mT to identify the origin of magnetic susceptibility. After demagnetization, AMS was measured using a Kappabridge KLY-3 (Table T1). Declinations of NRM after 20-mT cleaning were used for the reorientation of AMS axes by rotating to the present-day north.

SOURCE OF MAGNETIC SUSCEPTIBILITY

Volume magnetic susceptibility (K) and ARM are generally considered to be a measure of ferrimagnetic mineral concentration, although they show a grain size dependence (Maher, 1988). K is increased by fine superparamagnetic and coarse multidomain grains; conversely, ARM is increased by intermediate single-domain and pseudo-single-domain grains. K and ARM profiles at Site 1150 show nearly identical patterns (Fig. F2A). Both decrease sharply from the top of the hole to 200 mbsf and then vary from 10^{-5} to 10^{-6} kA/m for ARM and from 10^{-4} to 10^{-5} SI units for K .

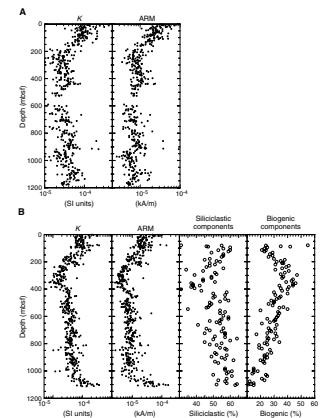
K and ARM profiles at Site 1151 also have a similar patterns. They quickly decrease from the top of the hole to 350 mbsf and then vary from 10^{-5} to 10^{-6} kA/m for ARM and from 10^{-4} to 10^{-5} SI units for K . Both profiles show a sharp increase below 1050 mbsf.

ARM and K in both holes reveal changes in the amounts of ferrimagnetic minerals. Figure F2B shows the comparison between the amounts of ferrimagnetic minerals and other components of sediments obtained by smear slide observation from Site 1151 (Sacks, Suyehiro, Acton, et al., 2000). Magnetic concentration is anticorrelated with biogenic components and is correlated with siliclastic components. This suggests that the magnetic minerals mainly originated from the siliclastic components and are also affected by the dilution of the biogenic components.

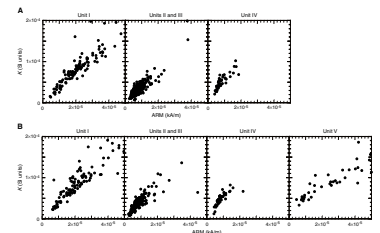
Because the magnetic susceptibility at Sites 1150 and 1151 is typically $<10^{-4}$ below 200 mbsf, the main source may be not only ferrimagnetic but also paramagnetic minerals (Tarling and Hrouda, 1993). In order to quantify the paramagnetic contribution to magnetic susceptibility, ARM vs. K for each lithologic unit is plotted in Figure F3. Each lithologic unit shows a similar distribution in both holes. Linear relationships between ARM and K are identified in all units at both sites. In Unit I at both sites, ARM increases with K , which indicates that variations in the amount of ferrimagnetic minerals dominate with little change in magnetic grain size. The distributions for Units II, III, and IV are more clustered than that of Unit I because they have lower variations in K and ARM. In Unit V at Site 1151, K is higher than ARM, but the nonzero intercept of data distribution suggests an important contribution of paramagnetic minerals. The data distribution also shows a wide variation in amounts of K and ARM.

Lithologic Unit I at both sites is characterized by large variations in ferrimagnetic mineral concentrations. Units II, III, and IV are characterized by lower and more constant concentrations of ferrimagnetic minerals. Unit V is characterized by relatively high K , with a significant paramagnetic contribution. Downhole profiles of ARM30/ARM (ARM30 = ARM after AF cleaning at 30 mT) show changes in the relative coercive force of the samples (Fig. F4). ARM30/ARM is fairly constant through Site 1150 and above 1050 mbsf at Site 1151. This suggests a similar ferrimagnetic mineral grain size. However, ARM30/ARM below 1050 mbsf (almost corresponding to Unit V) at Site 1151 shows higher coercive force, which indicates a different source of magnetic susceptibility.

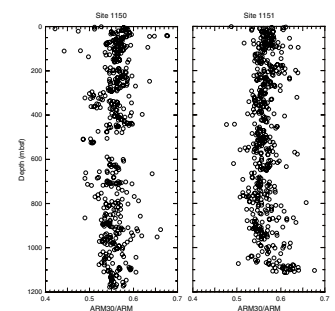
F2. K , ARM, and siliclastic and biogenic components, p. 10.



F3. K and ARM, p. 11.



F4. ARM30/ARM, p. 12.



MAGNETIC FABRIC

Coring Disturbance

The soft sediment obtained by the advanced hydraulic piston corer (APC) sometimes shows bowed bedding structures. If the bowing is extremely intense, the center of the halved core is also physically disturbed. In this case, it is expected that the magnetic fabric will show a K_{\min} axis deviating from the vertical axis of the core, whereas the undisturbed magnetic fabric will show a vertical K_{\min} . Because the beds in the center of the split core dip toward the core liner when deformed, the K_{\min} axis will shallow and tend toward the core liner for samples taken from split cores in the Ocean Drilling Program (ODP) core coordinate system. An example of this phenomenon is demonstrated in Figure F5A for cores from Hole 898A, which were recovered with the APC system and show severe bowing structures. K_{\min} directions in the core coordinate system are biased toward shallow dips and declination (180° in the ODP standard core coordinate system) (data from Kanamatsu, 1996). K_{\min} directions recovered from APC cores from Sites 1150 and 1151 are plotted in the core coordinate system (Fig. F5B, F5C), demonstrating that the directions are not biased. There are smaller disturbances caused by APC coring in the center of cores at Sites 1150 and 1151.

Downhole AMS Parameters

Downhole profiles of L , F , and K_{\min} inclination in each hole are shown in Figure F6A and F6B. At Site 1150, the parameter L is relatively uniform, ranging from 1.00 to 1.02, although several horizons show higher L values up to 1.04. No linear downcore increase is observed in F values. The F values at a depth of 300 mbsf in both holes are slightly higher then decrease slightly downhole. K_{\min} inclinations can be divided into two domains. The upper domain, above 500 mbsf, shows diversified K_{\min} inclinations ranging from 50° to 90° , but below 600 mbsf K_{\min} inclinations are slightly more concentrated, between 60° and 90° .

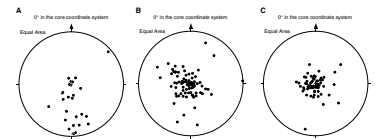
At Site 1151, the L values are relatively small. F values at ~ 300 mbsf are higher and then decrease downward with fluctuations. F values below 1100 mbsf are smaller and extremely clustered. K_{\min} inclinations show a wide dispersion in the upper depth. They become gradually more clustered downhole until 600 mbsf. Then K_{\min} inclinations become slightly shallower from 700 mbsf downhole.

Comparison between AMS and Fault and Bedding Structures

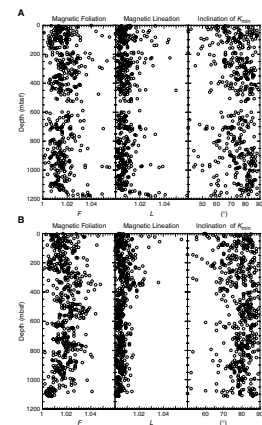
Site 1150

The frequency of faults and joints increases from Cores 186-1150B-1R through 50R (Sacks, Suyehiro, Acton, et al., 2000). The intervals at 900–1000 and 1100–1200 mbsf have especially high fault populations (Fig. F7). L and F values are higher in these intervals. Inclinations of K_{\min} are also scattered in these intervals. To compare planes of faults and joints and reoriented magnetic foliation, the poles and planes were plotted in Figure F8. Planes of faults and joints in the interval between 962 and 985 mbsf dominantly dip toward east-southeast and west-

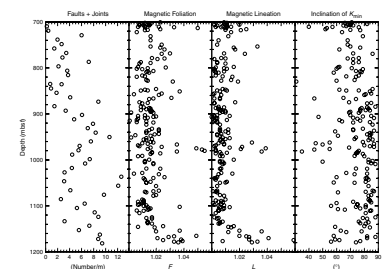
F5. K_{\min} directions for APC cores, p. 13.



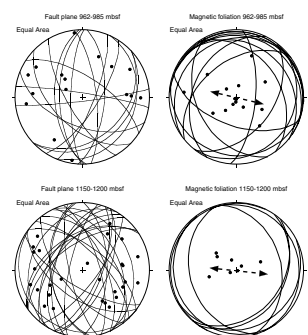
F6. L , F , and K_{\min} inclinations, p. 14.



F7. Faults and healed fractures, L , F , and K_{\min} inclinations, p. 15.



F8. Reoriented F and fault planes, p. 16.



northwest. The K_{\min} axis distribution tends to spread toward east-west directions from the pole of the stereonet. Planes of magnetic foliation, which are perpendicular to the K_{\min} axes, dip in the range of 3°–67°. Fault and joint planes are east-southeast and northwest-north-dipping in the interval between 1150 and 1200 mbsf. Inclinations of K_{\min} in this interval indicate dips of 2°–34° smaller, again spreading toward east-southeast and west-northwest directions. The magnetic fabric in the intervals that contain frequent faults and joints is inclined dipping magnetic foliation, whereas the magnetic fabric in the intervals containing few faults and joints shows fairly flat magnetic foliation (Fig. F7).

Site 1151

The tilt of bedding planes in Hole 1151A was observed below 900 mbsf, although the bedding is nearly horizontal above this depth (Sacks, Suyehiro, Acton, et al., 2000). Below 900 mbsf, most bedding planes dip by >10°, increasing downhole. The reoriented dip azimuths of bedding planes point dominantly to the east. Above 900 mbsf, no dominant dip direction is evident. (Sacks, Suyehiro, Acton, et al., 2000). The dip of magnetic foliation, which is perpendicular to K_{\min} axis, changes exactly in correspondence to bedding planes from 800 to 960 mbsf (Fig. F9). Also, the reoriented K_{\min} declination indicates the eastward dipping of magnetic foliation. The magnetic foliation is strongly controlled by bedding planes in this interval. However, the plane of magnetic foliation below 960 mbsf is fairly horizontal, although the bedding dips are eastward in orientation (Fig. F10).

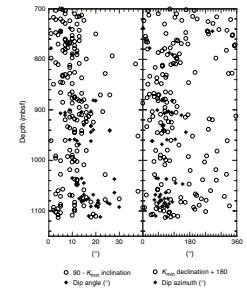
The number of faults and joints is highest in the intervals from 700 to 800 and from 1050 to 1100 mbsf (Fig. F11). The reoriented K_{\min} directions, especially declination, are scattered in these intervals. At 1050–1100 mbsf, K_{\min} inclinations would be expected to be 70° for a 20° bedding dip angle. But most K_{\min} inclinations show almost 90°. Smaller values of L and F are observed in this interval (Fig. F6B).

DISCUSSION AND SUMMARY

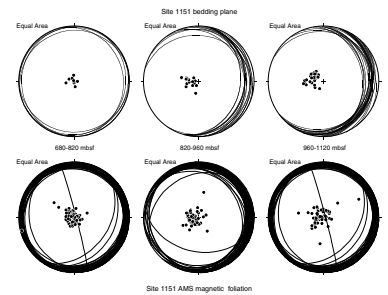
Magnetic foliation (F value) where structure is generally parallel to the bedding plane would be expected to increase downward because of compaction. This trend is observed in both holes to 500–600 mbsf. K_{\min} inclinations vary little and are generally steep (>60°). This indicates the formation of magnetic foliation parallel to bedding. Below 600 mbsf in both holes, the F value decreases slightly downward but most magnetic foliation remains parallel to the bedding plane. Higher values of L and F are observed in the intervals containing high numbers of faults and joints at Site 1150. The direction of magnetic foliation changes from the horizontal plane to oblique planes, which are closer to the planes of faults and joints. This suggests a grain fabric reorientation responding to a fault parallel local stress.

The magnetic fabric at Site 1151 shows a different pattern from that at Site 1150. Structures of magnetic fabric strongly reflect the bedding planes in the interval between 600 and 960 mbsf. Magnetic foliation inclines as bedding planes dip. The structure of the magnetic foliation is not concordant with the bedding plane below 960 mbsf, and anisotropy parameters in this interval are very small. The cause for this pattern is unclear, but it is possible that it is related to magnetic

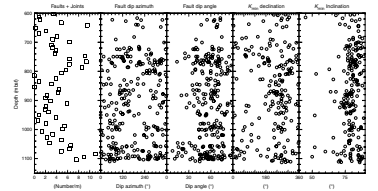
F9. Dip angle and azimuth of bedding planes and F , p. 17.



F10. Reoriented K_{\min} axes and bedding plane, p. 18.



F11. Fault dip azimuth and angle, K_{\min} inclination and reoriented declination, p. 19.



mineralogy because the sources of magnetic susceptibility are different than other units.

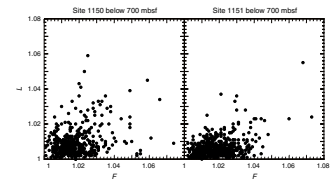
The magnetic fabric obtained from Sites 1150 and 1151 generally shows bedding parallel structure. The change of magnetic fabric in the upper domain is considered to be caused by compaction processes. The magnetic fabric in fault zones shows slightly larger L and F values. The directions of magnetic foliation seem to be affected by the fault plane structures. The comparison between parameters in at Sites 1150 and 1151 below 600 mbsf also demonstrates the possible fault effect on magnetic foliation (Fig. F12). The average F values at Site 1150, where the fault population is higher, are smaller than those at Site 1151.

The deformation structure obtained from the Japan Trench is characterized by small displacements of normal faults. The strain caused by tensional stress might be released completely only by fault displacement, with relatively insignificant modification of the grain fabric of sediment piles. The tensional stress at Sites 1150 and 1151 made a very small contribution to the change of magnetic fabric, although the systematic alteration of magnetic fabric is observed in the directions and parameters in the fault-developed intervals.

ACKNOWLEDGMENTS

We would like to thank Prof. Nobuaki Niitsuma for encouraging discussion and useful suggestions on this work. I thank my colleagues in the Deep Sea Research Department, Japan Marine Science and Technology Center (JAMSTEC) for support during the cruise and postcruise research. This research used samples and data provided by Ocean Drilling Program (ODP). ODP is sponsored by the U.S. National Science Foundation (NSF) and participating countries under management of Joint Oceanographic Institutions (JOI), Inc. Funding for this research was provided by JAMSTEC.

F12. Flinn-type diagram, p. 20.



REFERENCES

- Balsley, J.R., and Buddington, A.F., 1960. Magnetic susceptibility anisotropy and fabric of some Adirondack granites and orthogneisses. *Am. J. Sci.*, 2:6–20.
- Housen, B.A., and the ODP Leg 156 Scientific Party, 1996. Strain decoupling across the décollement of the Barbados accretionary prism. *Geology*, 24:127–130.
- Hounslow, M.W., 1990. Grain fabric measured using magnetic susceptibility anisotropy in deformed sediments of the Barbados accretionary prism: Leg 110. In Moore, J.C., Mascle, A., et al., *Proc. ODP, Sci. Results*, 110: College Station, TX (Ocean Drilling Program), 257–275.
- Jelinek, V., 1981. Characterization of the magnetic fabric of rocks. *Tectonophysics*, 79:63–67.
- Kanamatsu, T., 1996. Magnetic fabric analysis of fin-grained sediments, Iberia Abyssal Plain. In Whitmarsh, R.B., Sawyer, D.S., Klaus, A., and Masson, D.G. (Eds.), *Proc. ODP, Sci. Results*, 149: College Station, TX (Ocean Drilling Program), 335–342.
- Kanamatsu, T., Herrero-Bervera, E., and Taira, A., 2001. Magnetic fabrics of soft-sediment folded strata within a Neogene accretionary complex, the Miura group, central Japan, *Earth Planet. Sci. Lett.*, 187:333–343.
- Maher, B.A., 1988. Magnetic properties of some synthetic sub-micron magnetites. *Geophys. J. R. Astron. Soc.*, 94:83–96.
- Owens, W.H., 1993. Magnetic fabric studies of samples from Hole 808C, Nankai Trough. In Hill, I.A., Taira, A., Firth, J.V., et al., *Proc. ODP, Sci. Results*, 131: College Station, TX (Ocean Drilling Program), 301–310.
- Sacks, I.S., Suyehiro, K., Acton, G.D., et al., 2000. *Proc. ODP, Init. Repts.*, 186 [CD-ROM]. Available from: Ocean Drilling Program, Texas A&M University, College Station TX 77845-9547, USA.
- Shipboard Scientific Party, 2000a. Site 1150. In Sacks, I.S., Suyehiro, K., Acton, G.D., et al., *Proc. ODP, Init. Repts.*, 186, 1–209 [CD-ROM]. Available from: Ocean Drilling Program, Texas A&M University, College Station TX 77845-9547, USA.
- , 2000b. Site 1151. In Sacks, I.S., Suyehiro, K., Acton, G.D., et al., *Proc. ODP, Init. Repts.*, 186, 1–125 [CD-ROM]. Available from: Ocean Drilling Program, Texas A&M University, College Station TX 77845-9547, USA.
- Stacey, F.D., Joplin, G., and Lindsay, J., 1960. Magnetic anisotropy and fabric of some foliated rocks from S.E. Australia. *Geofis. Pura Appl.*, 47:30–40.
- Tarling, D.H., and Hrouda, F., 1993. *The Magnetic Anisotropy of Rocks*: London (Chapman and Hall).

Figure F1. Location of Leg 186 Sites 1150 and 1151. Contours are shown at 1000-m intervals landward of the Japan Trench.

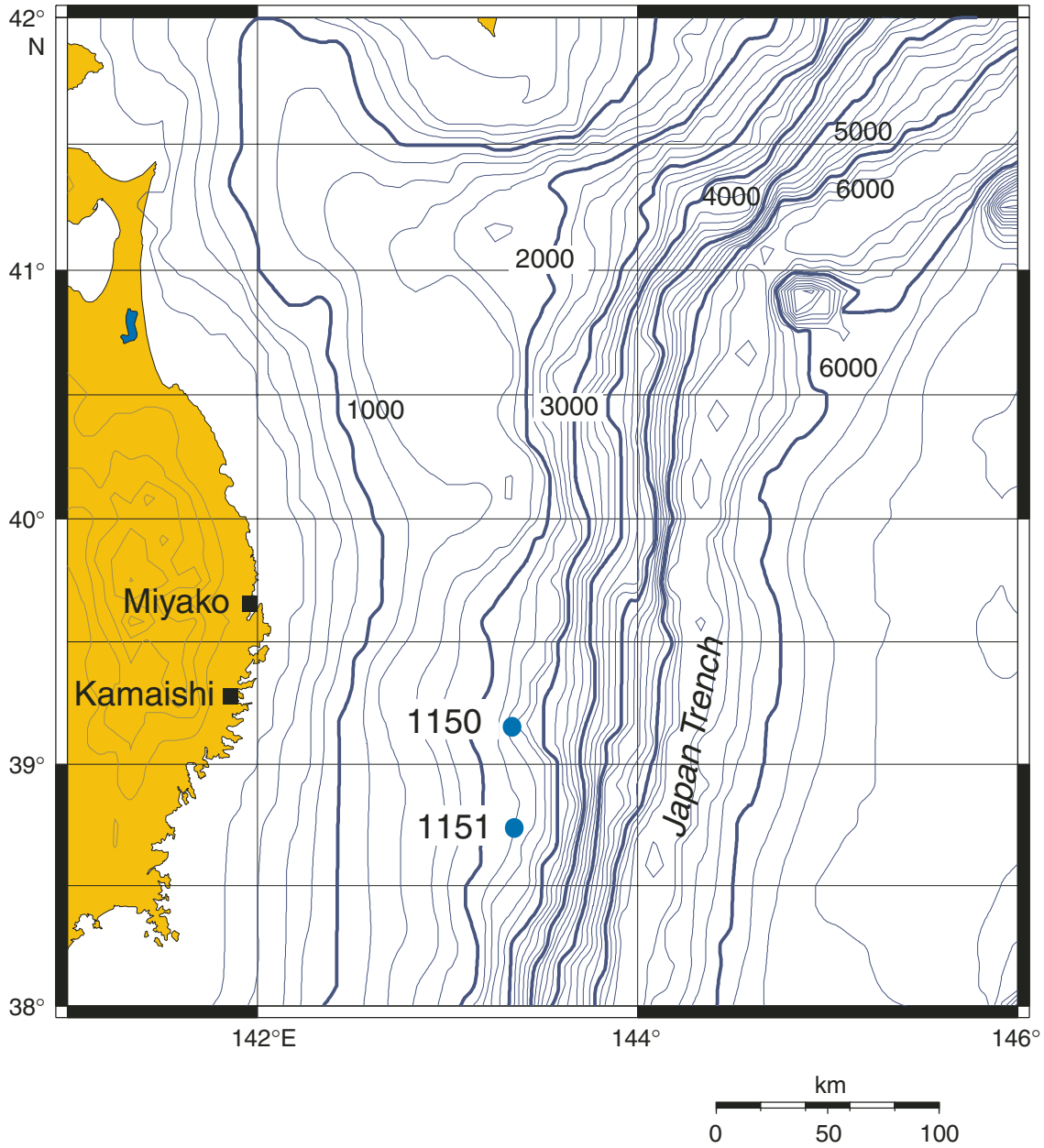


Figure F2. Downhole profiles of magnetic susceptibility (K) and anhysteretic remanent magnetization (ARM) at Sites (A) 1150 and (B) 1151, and siliclastic and biogenic components at Site 1151 (Sacks, Suyehiro, Acton, et al., 2000).

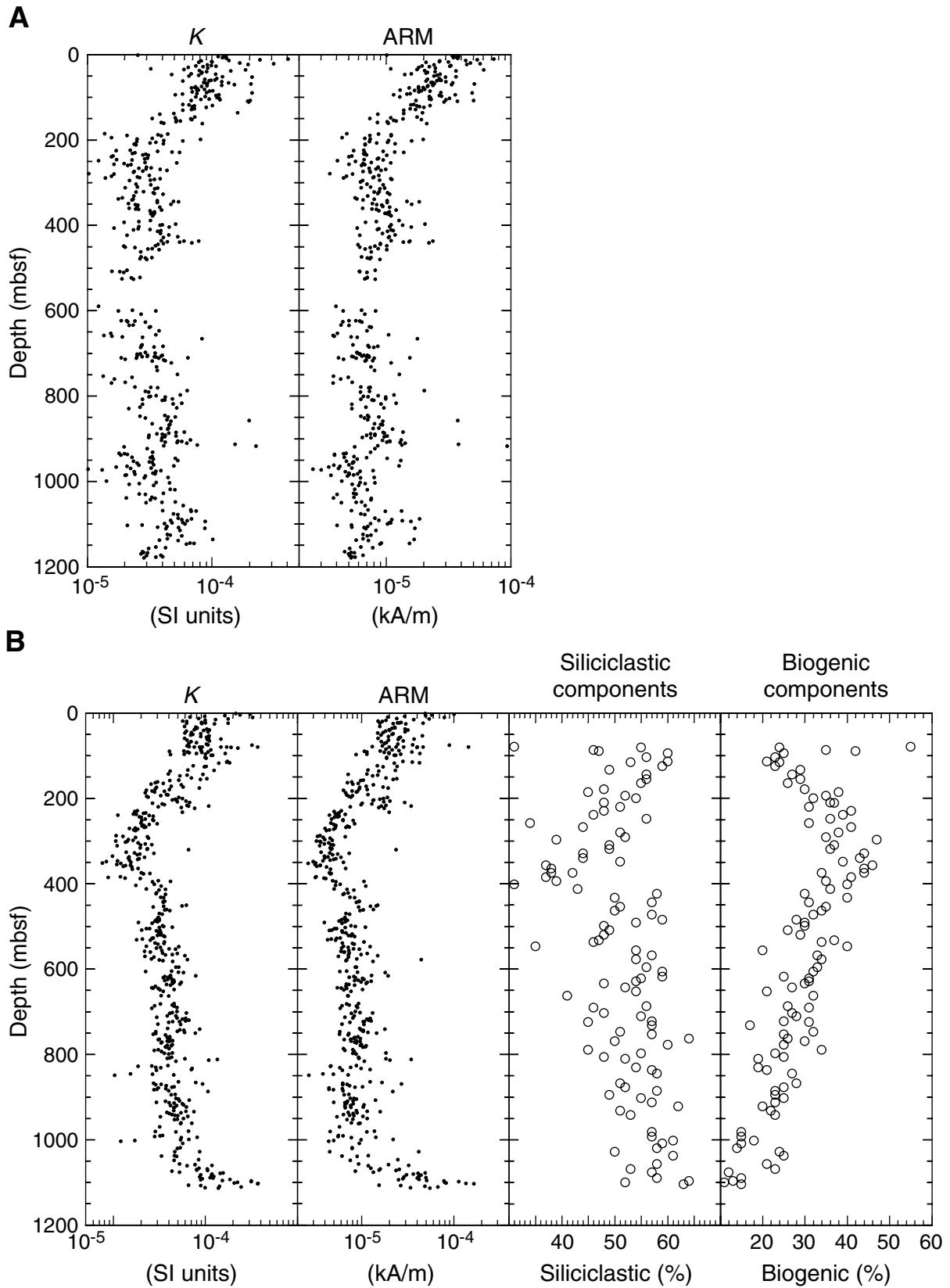


Figure F3. Variation of magnetic susceptibility (K) and anhysteretic remanent magnetization (ARM) at Sites (A) 1150 and (B) 1151.

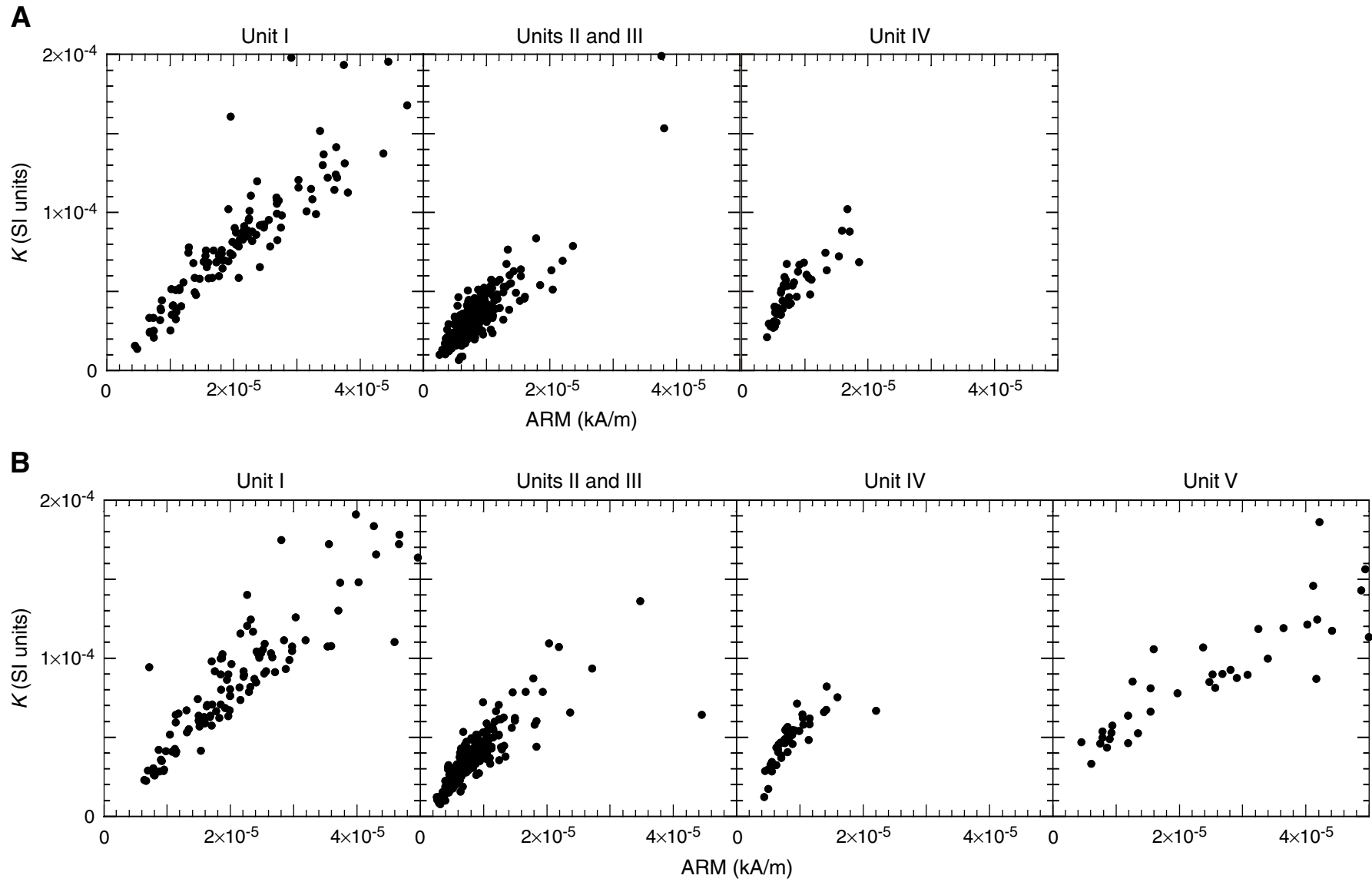


Figure F4. Downhole profiles of anhysteretic remanent magnetization (ARM)30/ARM (ARM30 = ARM after AF cleaning at 30 mT) at Sites 1150 and 1151.

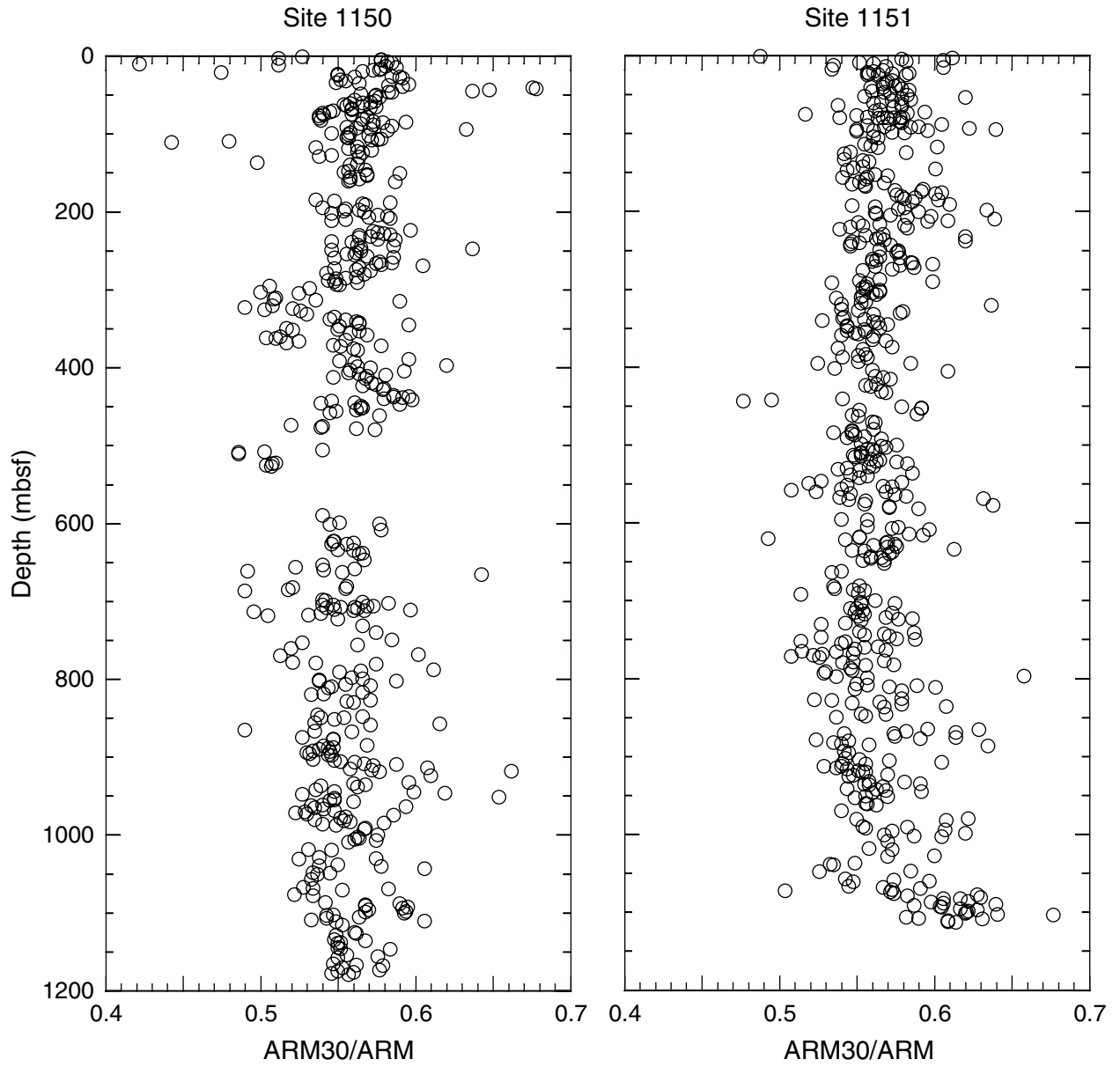


Figure F5. K_{\min} axis directions for APC cores. Equal-area lower hemisphere projection in core coordinate system. **A.** Hole 898A, magnetic foliation of bowing core. **B.** Hole 1150B. **C.** Hole 1150C.

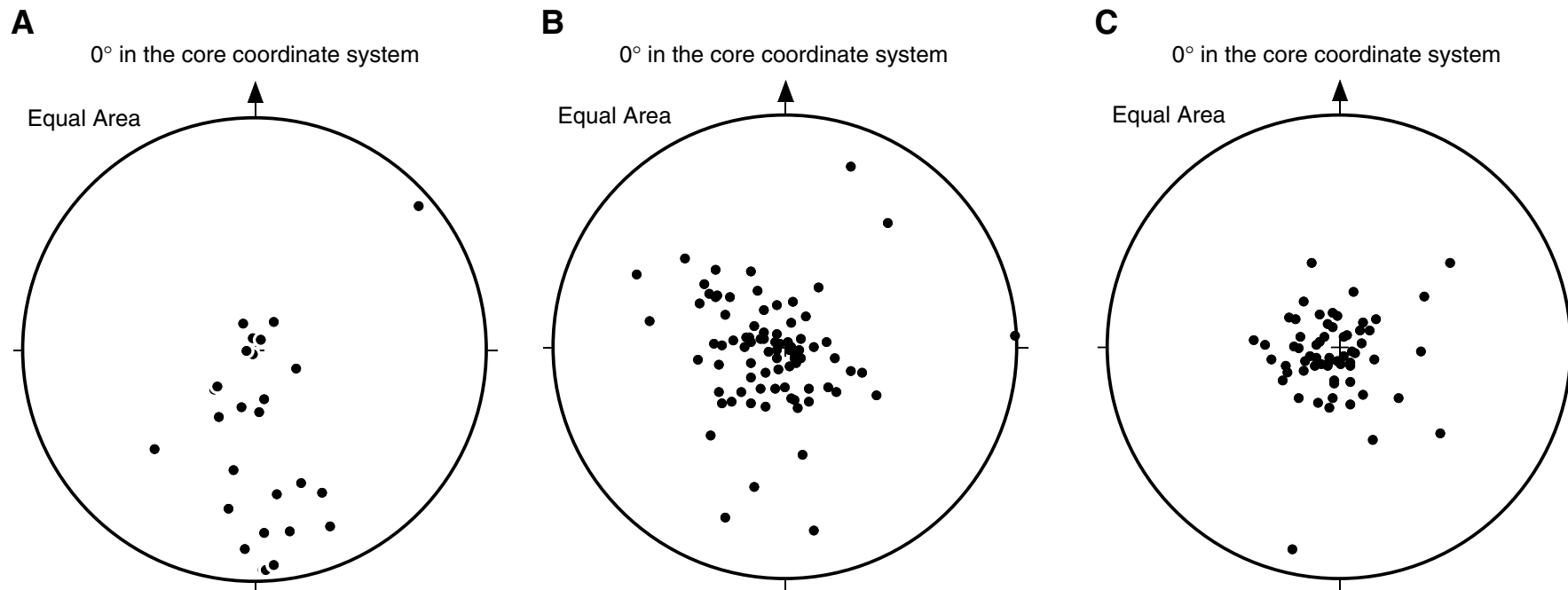


Figure F6. Downhole profile of L (magnetic lineation), F (magnetic foliation), and K_{\min} inclinations at Sites (A) 1150 and (B) 1151.

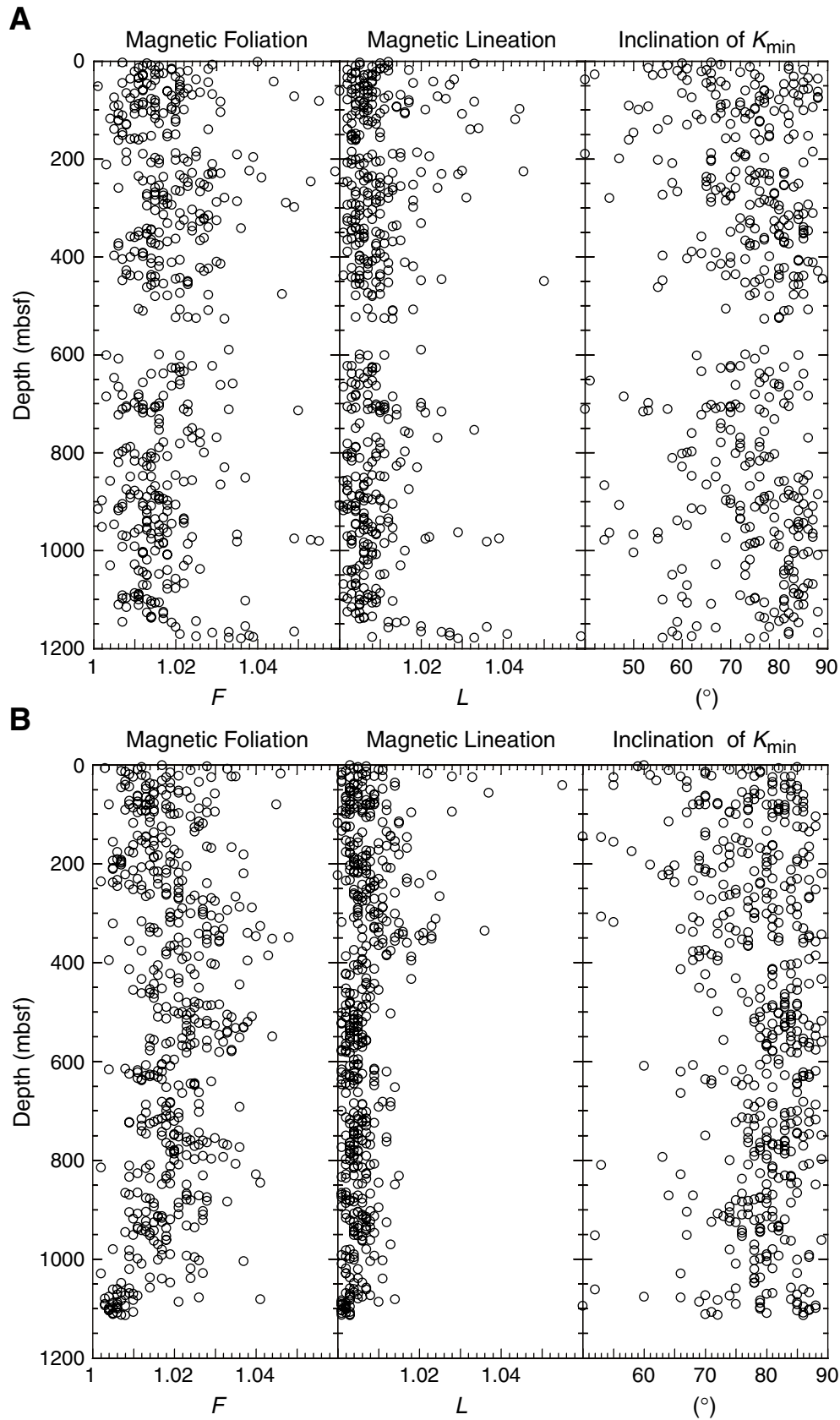


Figure F7. Downhole profiles of frequency of faults and healed fractures, L (magnetic lineation), F (magnetic foliation), and K_{\min} inclination in the interval 700–1200 mbsf, Site 1150.

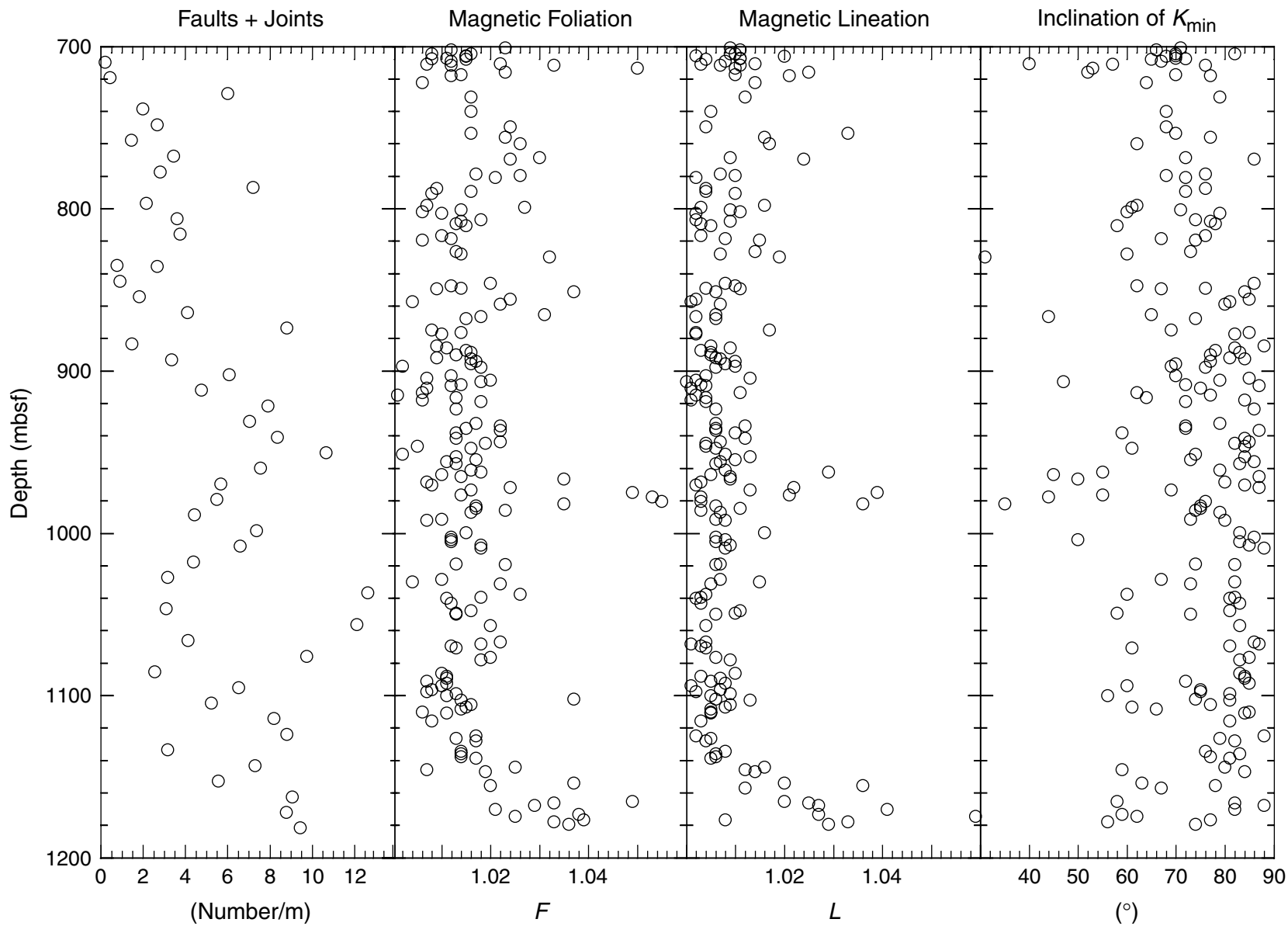


Figure F8. Plane of reoriented magnetic foliation and fault plane in the intervals 962–985 and 1150–1200 mbsf, Site 1150. Equal-area lower hemisphere projection after reorientation by paleomagnetic direction. Solid circles = K_{\min} axis, solid squares = pole of fault plane.

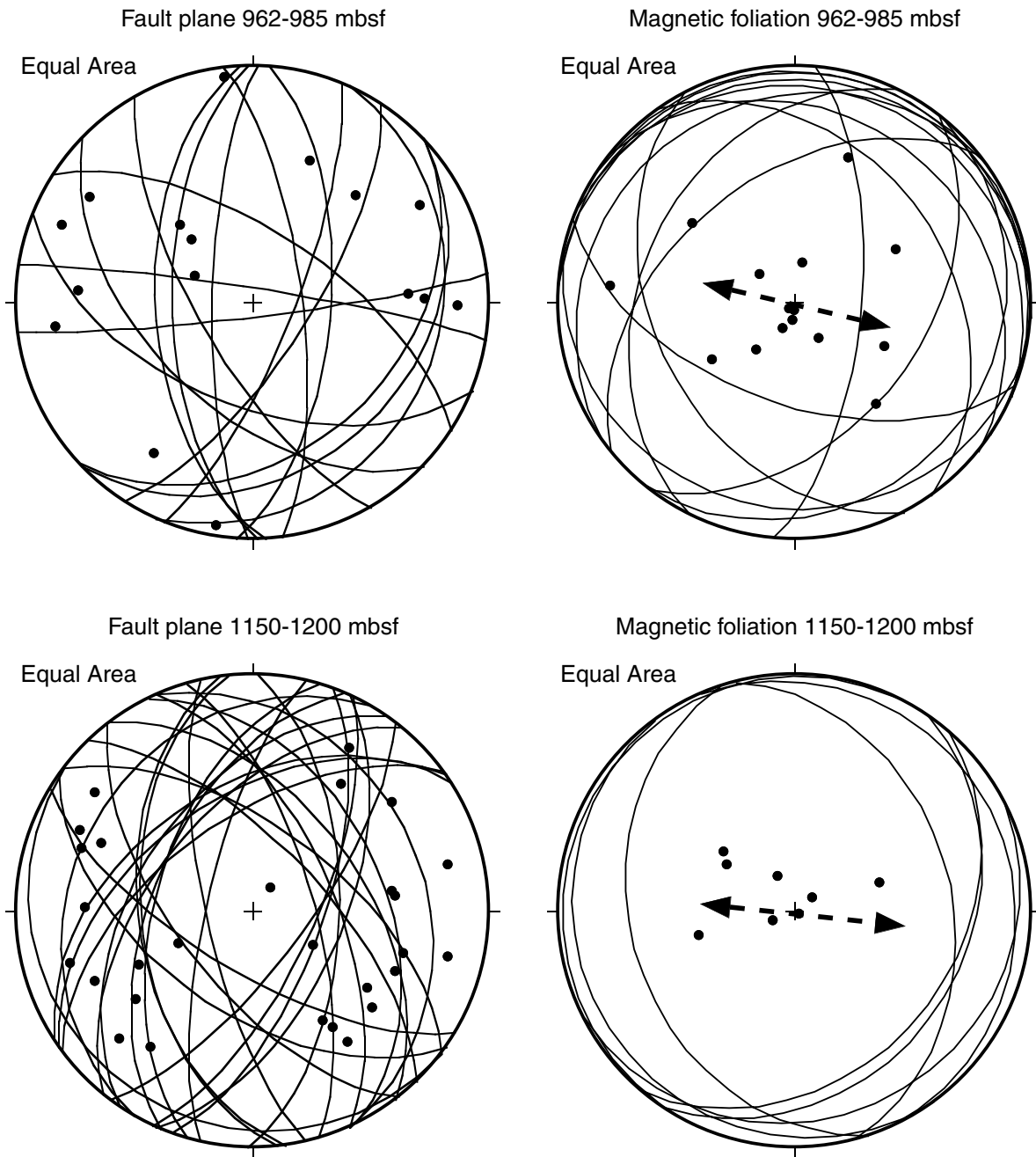


Figure F9. Dip angle of bedding plane and magnetic foliation and dip azimuth of bedding plane and reoriented magnetic foliation in the interval 700–1150 mbsf, Site 1151. Dip angle of magnetic foliation = $90^\circ - K_{\min}$ inclination, dip azimuth of magnetic foliation = K_{\min} declination + 180° .

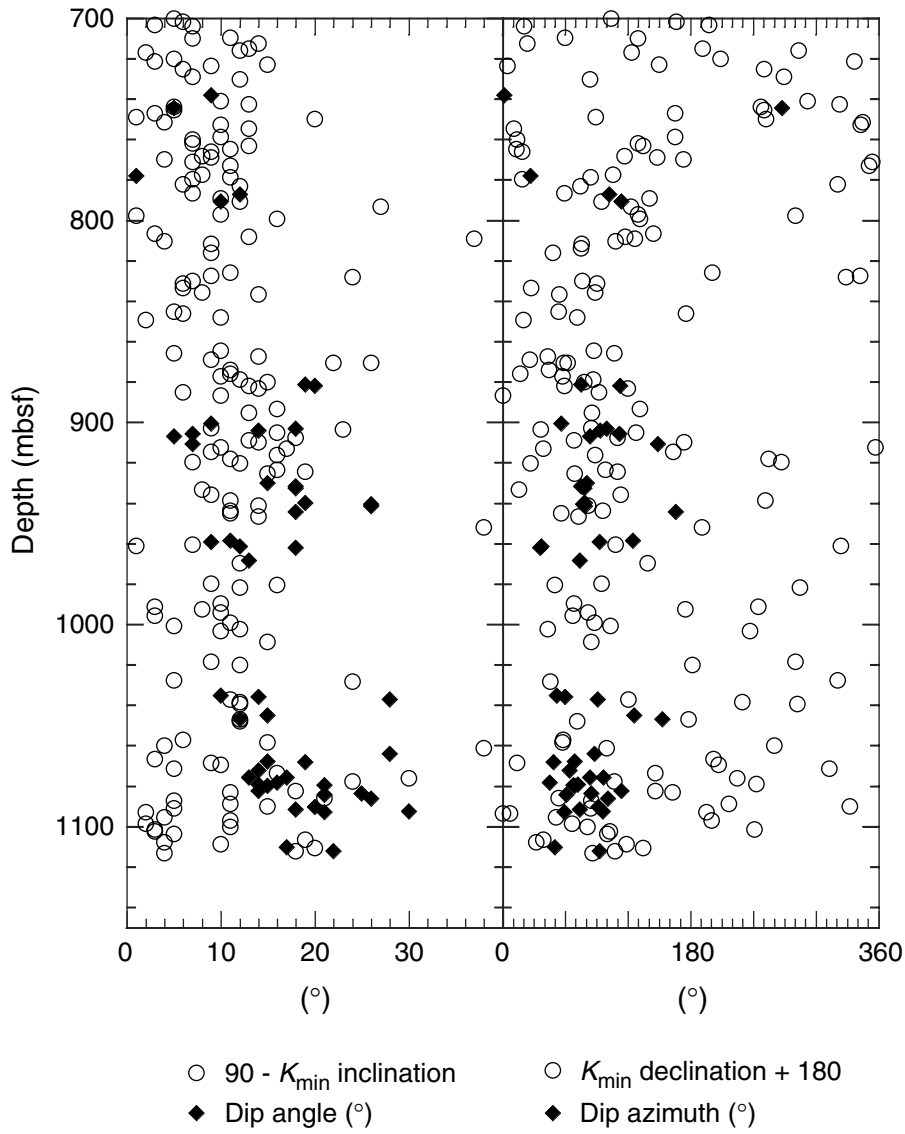


Figure F10. Equal-area hemisphere projection of reoriented K_{\min} axes and bedding plane in the intervals 680–820, 820–960, and 960–1120 mbsf, Site 1151. Directions were reoriented.

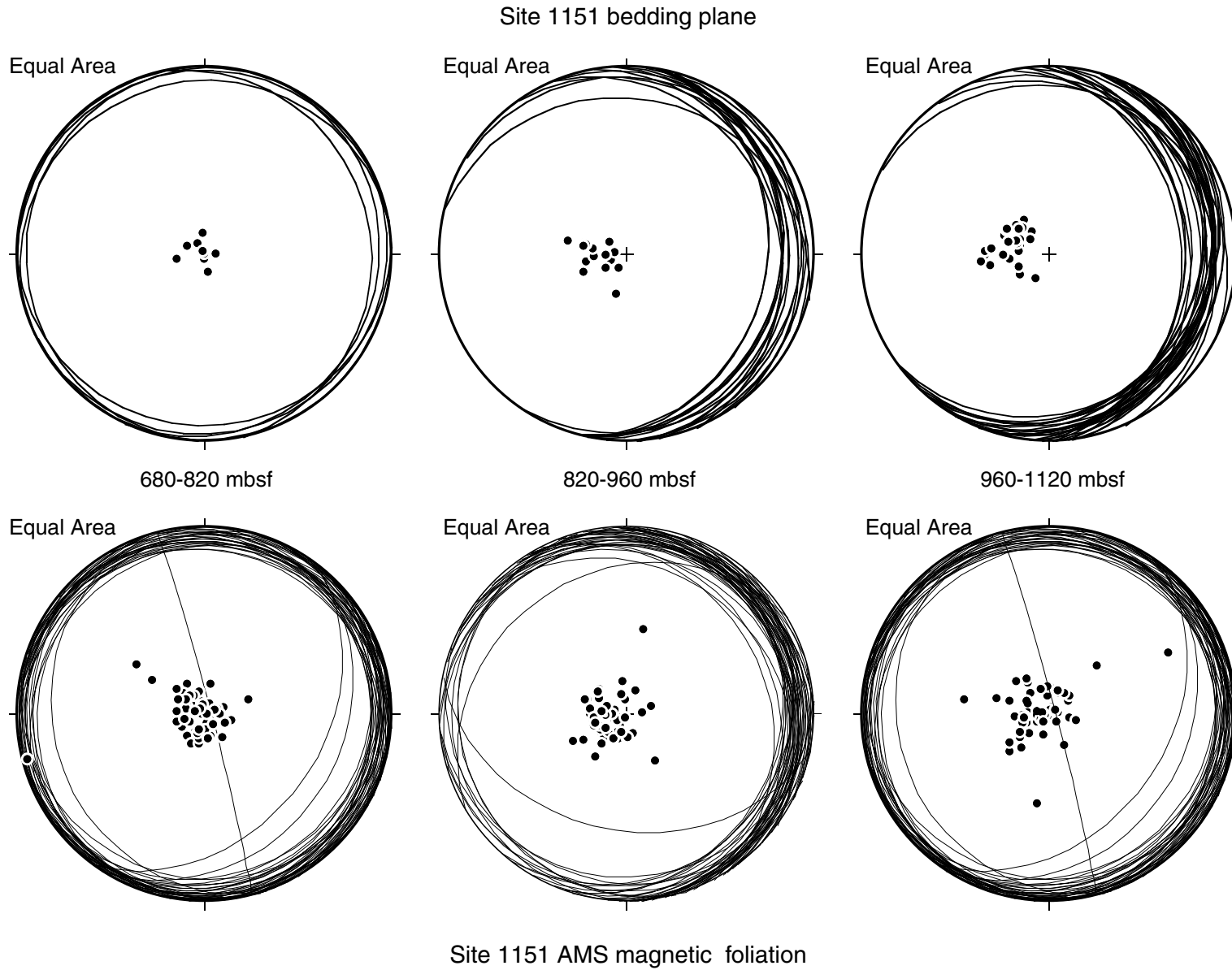


Figure F11. Downhole profiles of fault dip azimuth and angle and K_{min} inclination and reoriented declination in the interval between 600 and 1150 mbsf, Site 1151.

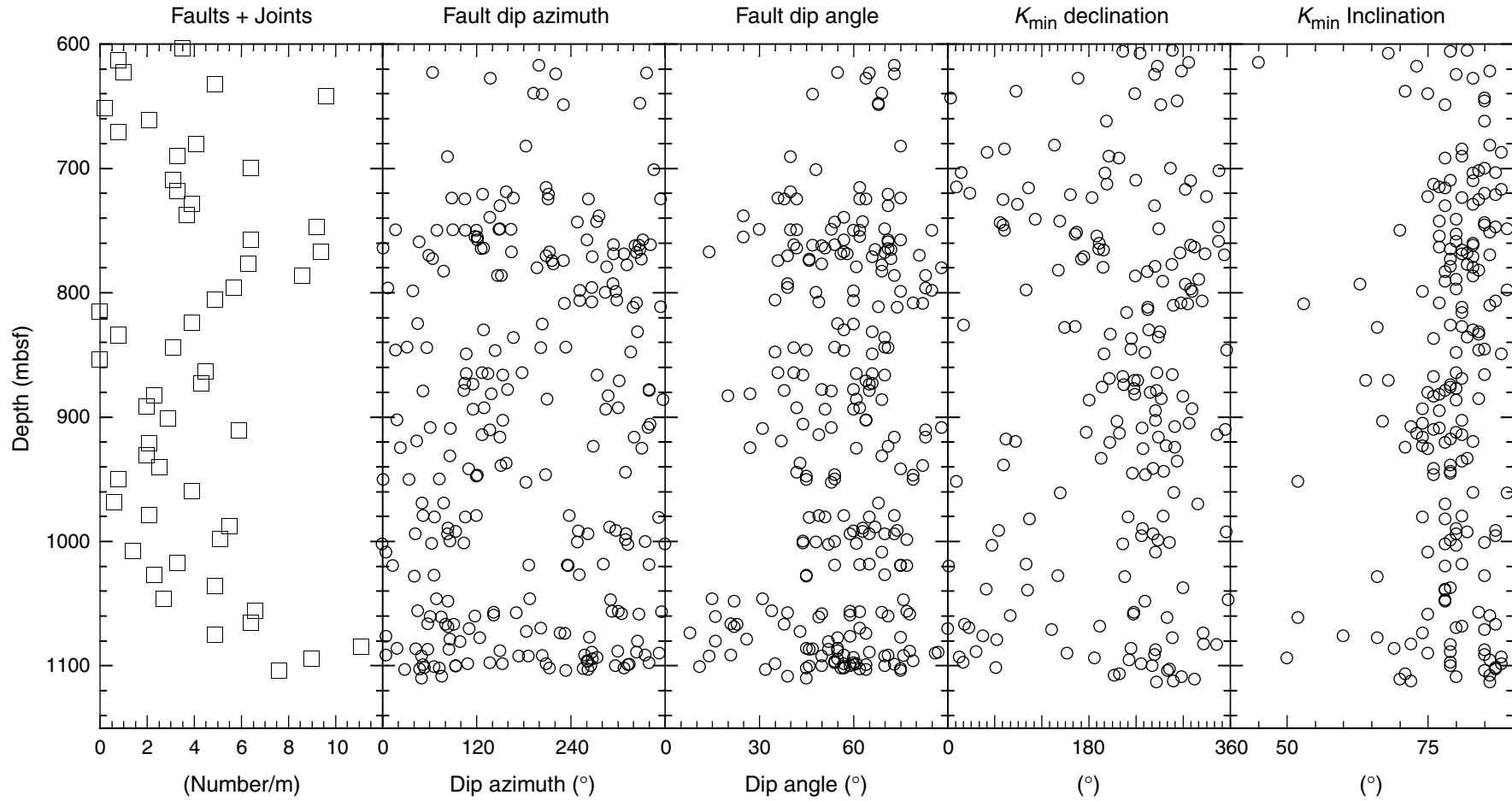


Figure F12. Flinn-type diagram below 700 mbsf at Sites 1150 and 1151.

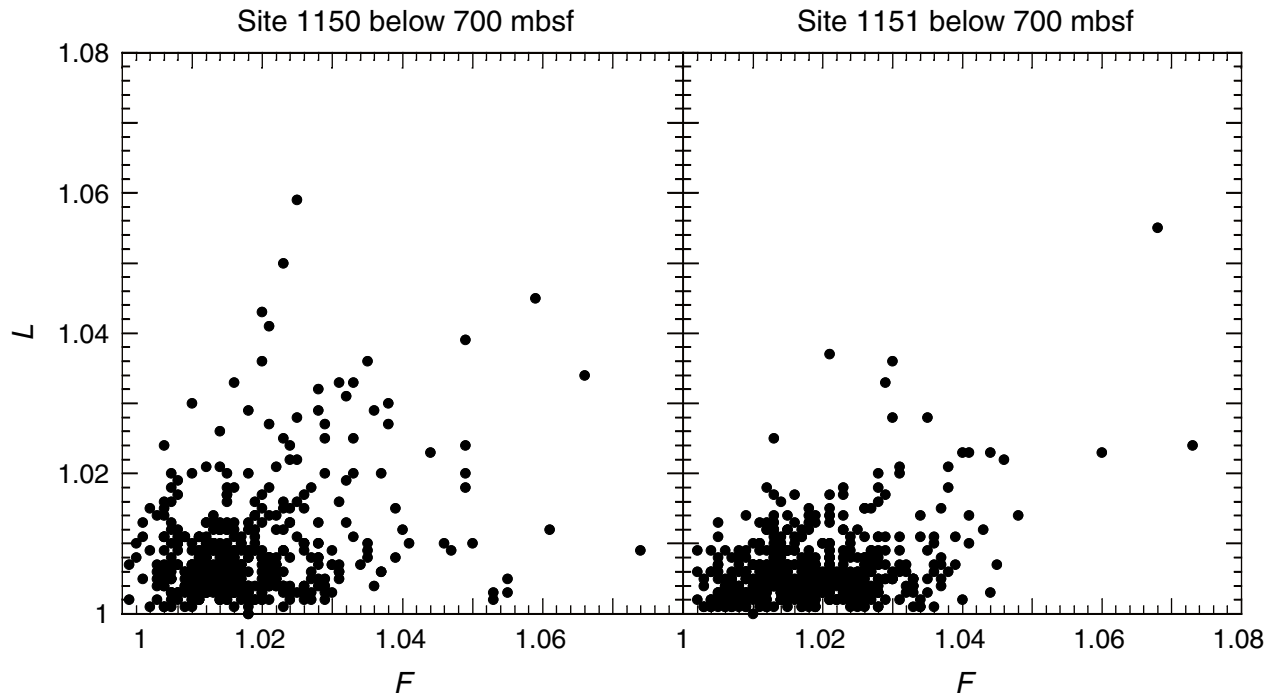


Table T1. AMS and paleomagnetic results.

Core, section, interval (cm)	Depth (mbsf)	Pmag (°)		Mean MS (SI units)	L	F	P'	K _{max} (°)		K _{int} (°)		K _{min} (°)	
		Inc.	Dec.					Dec.	Inc.	Dec.	Inc.	Dec.	Inc.
186-1150A- and 186-1150B-													
1H-1, 100-102	1	64.59	331.84	2.553-05	1.012	1.04	1.05	190	26	66	48	296	30
1H-2, 100-102	2.5	62.22	5.62	1.301-04	1.005	1.007	1.01	55	22	148	7	255	66
1H-3, 100-102	4	62.99	26.53	1.127-04	1.01	1.013	1.02	123	30	214	1	306	60
1H-4, 58-60	5.1	54.25	13.01	1.241-04	1.033	1.124	1.17	120	28	261	56	20	18
1H-5, 100-102	7	70.33	357.22	1.219-04	1.005	1.029	1.04	99	22	8	3	271	68
2H-1, 100-102	8.7	62.81	65.65	1.310-04	1.012	1.014	1.03	170	25	70	21	305	57
2H-2, 100-102	10.2	55.65	103.48	4.094-04	1.004	1.012	1.02	315	4	46	7	197	82
2H-3, 100-102	11.7	64.51	89.76	2.438-04	1.008	1.016	1.02	263	5	172	15	11	74
2H-4, 100-102	13.2	66.82	13.2	1.373-04	1.011	1.011	1.02	52	3	145	36	318	53
2H-5, 100-102	14.7	65.51	262.47	8.252-05	1.01	1.019	1.03	192	24	96	15	336	61
2H-6, 100-102	16.2	56.57	250.22	9.927-05	1.01	1.028	1.04	198	1	108	8	292	82
2H-7, 70-72	17.4	47.42	307.37	1.007-04	1.002	1.019	1.02	203	3	113	4	329	85
3H-1, 100-102	18.2	71.97	110.87	7.850-05	1.017	1.015	1.03	47	18	143	16	272	65
3H-2, 102-104	19.7	3.17	294.62	1.679-04	1.012	1.023	1.04	51	27	149	13	262	59
3H-3, 100-102	21.2	40.86	92.54	3.128-04	1.009	1.01	1.02	61	9	155	25	312	64
3H-4, 100-102	22.7	41.92	79.46	1.954-04	1.004	1.021	1.03	60	14	153	11	278	72
3H-5, 100-102	24.2	64.24	101.72	9.200-05	1.004	1.017	1.02	199	4	107	24	298	66
3H-6, 100-102	25.7	55.29	94.07	9.909-05	1.003	1.016	1.02	46	12	143	31	297	56
3H-7, 70-72	26.9	60.93	121.79	1.084-04	1.007	1.015	1.02	227	8	135	12	349	75
5H-1, 100-102	37.2	57.15	233.89	7.969-05	1.028	1.025	1.05	190	2	98	50	281	40
5H-2, 100-102	38.7	56.47	227.62	1.414-04	1.005	1.015	1.02	348	16	251	24	108	61
5H-3, 100-102	40.2	65.55	253.97	9.045-05	1.008	1.021	1.03	299	24	31	5	131	66
5H-4, 100-102	41.7	65.03	244.98	8.324-05	1.023	1.044	1.07	308	8	41	20	198	68
5H-5, 100-102	43.2	23.59	262.07	8.273-05	1.008	1.028	1.04	269	3	359	4	138	85
5H-6, 100-102	44.7	47.49	257.04	6.825-05	1.018	1.007	1.03	230	13	324	21	110	65
5H-7, 80-82	46	53.82	252.38	1.076-04	1.006	1.013	1.02	52	3	321	6	165	83
6H-1, 100-102	46.7	39.05	157.22	4.771-05	1.002	1.011	1.01	201	9	111	1	16	81
6H-2, 100-102	48.2	64.93	162.84	7.840-05	1.027	1.021	1.05	272	15	182	2	83	75
6H-3, 100-102	49.7	43.69	172.97	6.541-05	1.006	1.014	1.02	297	17	31	13	156	69
6H-4, 103-105	51.2	59.33	190.22	1.219-04	1.007	1.001	1.01	268	48	147	25	40	31
6H-6, 100-102	54	52.54	168.83	2.097-04	1.005	1.021	1.03	120	0	210	24	30	66
7H-1, 97-99	56.2	44.48	105.58	1.095-04	1.004	1.023	1.03	72	3	162	3	298	86
7H-2, 100-102	57.7	58.08	111.61	8.797-05	1.003	1.012	1.02	12	4	102	2	218	85
7H-3, 100-102	59.2	67.64	128.17	1.056-04	1.006	1.021	1.03	136	4	45	12	243	77
7H-4, 27-29	60	61.79	131.78	9.828-05	1.007	1.012	1.02	13	16	105	4	209	73
8H-1, 40-42	65.1	-25.52	234.39	8.595-05	1.003	1.008	1.01	178	53	356	37	87	1
8H-1, 100-102	65.7	50.57	196.82	1.367-04	1.007	1.01	1.02	255	2	345	6	145	83
8H-2, 100-102	67.2	57.57	185.47	9.214-05	1.004	1.029	1.04	112	12	21	3	278	78
8H-3, 101-103	68.7	53.59	164.01	2.060-04	1.015	1.024	1.04	318	7	50	21	211	67
9H-1, 100-102	75.2	-23.93	175.3	7.396-05	1.011	1.009	1.02	272	2	2	1	128	88
9H-2, 107-109	76.8	17.05	124.66	7.316-05	1.026	1.014	1.04	263	9	171	10	34	77
9H-3, 100-102	78.2	-29.71	155.06	6.882-05	1.002	1.02	1.03	194	3	285	10	90	80
9H-4, 105-107	79.7	12.17	165.12	7.631-05	1.017	1.015	1.03	292	7	38	66	199	23
9H-5, 100-102	81.2	51.72	17.96	8.730-05	1.005	1.055	1.07	57	10	149	10	284	76
9H-6, 100-102	82.7	-49.34	229.64	7.790-05	1.033	1.031	1.07	276	35	56	48	171	21
9H-7, 80-82	84	-40.31	187.09	7.601-05	1.017	1.02	1.04	296	4	205	5	65	84
10H-1, 60-62	84.3	80.79	235.98	1.020-04	1.006	1.012	1.02	58	8	326	16	173	72
10H-2, 96-98	85.3	19.7	111.55	9.602-05	1.006	1.015	1.02	43	6	135	11	284	77
10H-3, 101-103	86.9	-37.28	298.84	6.958-05	1.004	1.011	1.02	314	21	224	0	133	69
10H-4, 100-102	88.3	-49.79	182.54	9.060-05	1.008	1.012	1.02	212	12	118	18	334	68
11H-1, 100-102	94.2	54.04	164.09	1.143-04	1.006	1.015	1.02	108	10	15	20	224	68
11H-2, 100-102	95.7	48.42	156.88	1.078-04	1.007	1.01	1.02	297	4	28	15	192	75
11H-3, 97-99	97.2	-8.52	181.57	5.137-04	1.044	1.114	1.17	194	1	104	9	288	81
11H-4, 73-75	98	-50.88	22.67	8.880-05	1.011	1.019	1.03	119	12	211	7	331	75
11H-5, 105-107	99.1	-31.11	193.09	7.461-05	1.021	1.022	1.04	272	9	9	38	171	51
11H-6, 100-102	100.5	30.36	40.07	1.105-04	1.007	1.02	1.03	241	4	332	3	102	85
11H-7, 130-132	102.2	70.31	29.5	1.149-04	1.004	1.014	1.02	126	0	36	11	217	79
12H-1, 119-121	103.9	-37.36	40.84	9.516-05	1.016	1.031	1.05	6	14	273	10	150	73
12H-2, 43-45	104.6	-27.77	265.48	8.189-05	1.006	1.012	1.02	320	16	52	9	170	71
12H-3, 84-86	106.2	6.84	313.32	1.158-04	1.01	1.017	1.03	354	22	263	2	168	68
12H-4, 3-5	106.9	-10.87	329.58	6.849-05	1.016	1.006	1.02	95	8	356	51	192	38
12H-4, 71-73	107.5	19.53	21.65	2.037-04	1.03	1.01	1.04	7	13	99	10	227	74
12H-5, 90-92	109.2	46.52	296.78	1.932-04	1.005	1.015	1.02	79	22	343	14	224	63
12H-6, 92-94	110.6	-39.87	317.56	1.979-04	1.003	1.007	1.01	158	7	68	1	329	82

Notes: MS = magnetic susceptibility. Inc. = inclination, Dec. = declination. Only a portion of this table appears here.
 The entire table is available in [ASCII](#).